ACS Infectious Diseases

pubs.acs.org/journal/aidcbc

Article

Anti-Intracellular MRSA Activity of Antibiotic-Loaded Lipid-Polymer Hybrid Nanoparticles and Their Effectiveness in Murine Skin Wound Infection Models

Wenrui Li,[¶] Chuan Hao Tan,[¶] Jong-Suep Baek, Lai Jiang, Noele Kai Jing Ng, Kelvin Kian Long Chong, Jun Jie Wong, Liheng Gao, Kimberly A. Kline, and Say Chye Joachim Loo*

Cite This: https://doi.org/10.1021/acsinfecdis.4c01016

Read Online

ACCESS | Metrics & More | Article Recommendations | Supporting Information

Downloaded via Say Chye (Joachim) Loo on February 14, 2025 at 07:16:15 (UTC).
See https://pubs.acs.org/sharingguidelines for options on how to legitimately share published articles.

ABSTRACT: Methicillin-resistant *Staphylococcus aureus* (MRSA) is a significant concern for skin and soft tissue infections. Apart from biofilm formation, these bacteria can reside intracellularly in phagocytic and nonphagocytic mammalian cells, complicating treatment with conventional antibiotics. Lipid-polymer hybrid nanoparticle (LPN) systems, combining the advantages of polymeric nanoparticles and liposomes, represent a new generation of nanocarriers with the potential to address these therapeutic challenges. In this study, gentamicin (Gen) and vancomycin (Van) were encapsulated in LPNs and evaluated for their ability to eliminate intracellular MRSA in phagocytic macrophage RAW-Blue cells and nonphagocytic epithelial HaCaT cells. Compared to free antibiotics at 100 μg/mL, LPN formulations significantly reduced intracellular bacterial loads in both cell lines. Specifically, LPN-Van resulted in approximately 0.7 Log CFU/well reduction in RAW-Blue cells and 0.3 Log CFU/well reduction in HaCaT cells. LPN-Gen showed a more pronounced reduction, with approximately 1.26 Log CFU/well reduction in RAW-Blue cells and 0.45 Log CFU/well reduction in HaCaT cells. In vivo, LPN-Van at 500 μg/mL significantly reduced MRSA biofilm viability compared to untreated controls ($p < 0.001$), achieving 98% eradication based on median values. In comparison, free vancomycin achieved a nonstatistically significant 79.2% reduction in biofilm viability compared to control. Prophylactically, LPN-Van at 500 μg/mL decreased MRSA levels to the limit of detection, resulting in a ~3.5 Log reduction in the median CFU/wound compared to free vancomycin. No acute dermal toxicity was observed for LPN-Van based on histological analysis. These data indicate that LPNs show promise as a drug delivery platform technology to address intracellular infections.

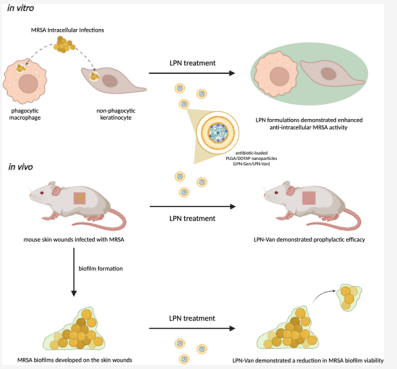

KEYWORDS: *lipid-polymer hybrid nanoparticle (LPN), methicillin-resistant Staphylococcus aureus (MRSA), intracellular infections, skin wound infection model, drug delivery*

The Gram-positive bacterial pathogen, *Staphylococcus aureus*, is a leading cause of skin and soft tissue infections with varying severities.[1] Once considered strictly extracellular, *S. aureus* is now recognized as facultative intracellular, capable of invading and surviving in phagocytic and nonphagocytic mammalian cells.[2] In professional phagocytes, *S. aureus* produces diverse evasion molecules that counteract host antimicrobial defenses, including detoxifying enzymes against reactive oxygen species,[3] factors that neutralize antimicrobial peptides[4] and lysozyme,[5] and systems that maintain bacterial survival under acidic pH conditions.[6] In nonprofessional phagocytes, *S. aureus* employs a zipper-like mechanism of invasion, using fibronectin-binding proteins to recruit host fibronectin and engage integrins, facilitating bacterial internalization.[7]

Beyond intracellular persistence, *S. aureus* utilizes biofilm formation as an additional survival strategy, readily establishing biofilms on medical implants[8] and in chronic wounds.[9] The emergence of methicillin-resistant *S. aureus* (MRSA) strains has further complicated treatment. Community-associated MRSA (CA-MRSA), exemplified by strains like USA300, spreads among healthy individuals without predisposing risk factors.[10] Current standard protocols for MRSA treatment typically involve vancomycin or daptomycin as first-line therapies.[11] However, these treatments show limited effectiveness against bacteria residing in intracellular and biofilm niches due to the prevalence of diverse resistance mechanisms.[12,13] These protected niches serve as reservoirs for recurring infections, contributing to the frequent relapse of MRSA infections despite prolonged treatment.

To enhance antibiotic efficacy against these persistent infections, engineering approaches have been investigated. Polymeric nanocarriers, particularly those based on biodegrad-

Received: December 20, 2024
Revised: February 7, 2025
Accepted: February 7, 2025

© XXXX American Chemical Society

Table 1. Physical Properties of Antibiotic-Loaded PLGA and PLGA/DOTAP Nanoparticles[a]

formulations	particle size (nm)	polydispersity index	zeta potential (mV)	encapsulation efficiency (%)
vancomycin (PLGA)	103.7 ± 6.9	0.134 ± 0.012	−20.1 ± 2.4	41.7 ± 5.8
vancomycin (PLGA/DOTAP)	124.8 ± 7.8	0.190 ± 0.015	15.3 ± 3.1	68.5 ± 7.9
gentamicin (PLGA)	105.7 ± 4.7	0.112 ± 0.005	−24.1 ± 4.3	38.6 ± 7.1
gentamicin (PLGA/DOTAP)	122.7 ± 11.5	0.195 ± 0.016	16.5 ± 3.2	63.9 ± 6.2

[a]Nanoparticle batches were prepared in triplicate, and characterization analyses were performed in duplicate for each batch.

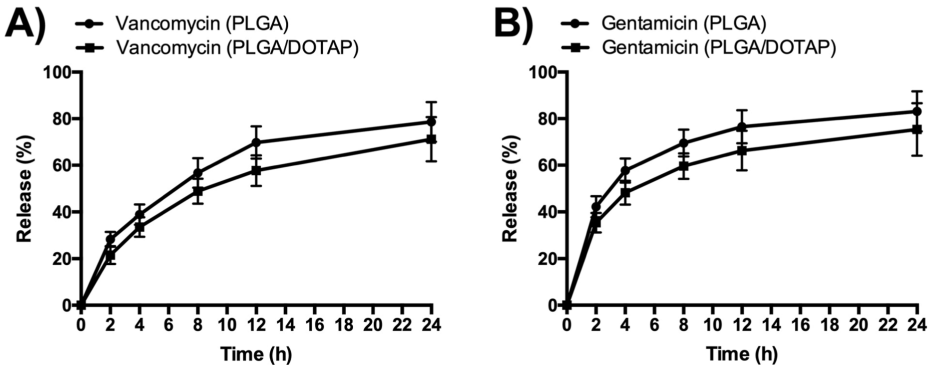

Figure 1. Release profiles of vancomycin (A) and gentamicin (B) from PLGA (circles) and PLGA/DOTAP (squares) nanoparticles. The release was evaluated in PBS (pH 7.4) for 24 h at 37 °C (n = 5, mean ± SD).

able polymers such as poly(lactic-*co*-glycolic acid) (PLGA) and poly(ε-caprolactone) (PCL),[14,15] offer controlled degradation rates and versatile surface modification options. For instance, PLGA-based formulations loaded with gentamicin demonstrated efficacy against intracellular *Klebsiella pneumoniae* infections.[16] Similarly, liposomes, the first nanocarriers to receive FDA approval, have shown promise in enhancing antibiotic delivery to *S. aureus* biofilms.[17] Their effectiveness stems from their ability to merge with bacterial membranes, enabling direct delivery of therapeutic agents to bacterial cells.

However, clinical translation of these single-component carrier systems faces significant challenges. Liposome-based vehicles are susceptible to instability postadministration due to disruption by plasma proteins and mechanical stress, compromising their structural integrity and physicochemical properties.[18] Additionally, these systems often exhibit burst release profiles,[19] resulting in premature and uncontrolled release of the therapeutic payload before reaching the target site. On the other hand, polymeric nanoparticles face suboptimal drug loading efficiencies and rapid clearance from systemic circulation,[20] limiting their intracellular antibiotic delivery.

To overcome these limitations, lipid-polymer hybrid nanoparticles (LPNs) have emerged as a promising platform, combining the advantages of both carrier types.[21] LPNs typically consist of a biodegradable polymeric core that provides mechanical stability and controlled drug release, surrounded by a lipid shell that enhances biocompatibility and facilitates interactions with cell membranes. This dual-component structure enables efficient bacterial targeting and sustained drug release, enhancing antibiotic efficacy against planktonic and biofilm-associated bacteria.[22]

Building upon our proof-of-concept study using a protozoan surrogate model for *Enterococcus faecalis* infection,[23] this study represents a significant advancement by targeting MRSA, a pathogen notorious for its antibiotic resistance and intracellular persistence. While the scientific community has made progress in antibiotic delivery and biofilm disruption,[24] the challenge of targeting intracellular MRSA across different cell types remains largely unexplored. In this study, we investigated the therapeutic potential of LPNs for treating intracellular MRSA infections across two distinct cell types: murine macrophages and human keratinocytes. This approach provides a comprehensive understanding of the treatment's effectiveness in both professional and nonprofessional phagocytes, addressing the critical challenge of eradicating bacteria within protected intracellular niches. To extend the translational relevance of the findings, we evaluated the efficacy of LPNs in an in vivo mouse skin wound infection model, demonstrating both preventive and therapeutic effectiveness against MRSA infections. This translational aspect underscores the clinical relevance of our approach, moving beyond in vitro studies to provide a robust preclinical evaluation.

RESULTS AND DISCUSSION

Characterization of Antibiotic-Loaded PLGA/DOTAP Nanoparticles. This study focused on the development of LPNs loaded with the aminoglycoside gentamicin (Gen) and the glycopeptide vancomycin (Van) for treating MRSA. While CA-MRSA is generally susceptible to gentamicin,[25] vancomycin remains the first-line treatment for systemic MRSA infections.[11] The antibiotics were encapsulated individually into LPNs using the emulsion-evaporation method.

Incorporating the cationic lipid DOTAP into the PLGA nanoparticles increased the particle size by approximately 20 nm compared to pure PLGA nanoparticles (Table 1). The positive zeta potential observed for LPNs confirmed the successful coating of the polymeric core with the lipid layer. This lipid coating enhances the likelihood of nanoparticle interaction with cell surfaces, facilitates internalization, and significantly improved the encapsulation efficiency. Transmission electron microscopy images supporting the core−shell structure of LPNs were previously documented in our research.[23] All formulations exhibited a narrow nanoparticle size distribution with a Polydispersity Index (PDI) of less than 0.2.

https://doi.org/10.1021/acsinfecdis.4c01016
ACS Infect. Dis. XXXX, XXX, XXX−XXX

Hydrophobic drugs typically interact well with PLGA matrices, whereas amphiphilic and hydrophilic drugs exhibit weaker interactions, often resulting in lower encapsulation efficiency and faster release.[26] However, the addition of the cationic lipid DOTAP enables hydrophilic drugs (e.g., gentamicin and vancomycin) to be condensed between the lipid layer and the PLGA matrix,[22] thereby improving encapsulation efficiency and achieving a more sustained release profile (Figure 1). These findings are consistent with previous studies demonstrating that cationic lipids can enhance the retention of hydrophilic drugs within nanoparticle systems.[22,27]

In Vitro antiMRSA Activity of LPN-Encapsulated Antibiotics. Table 2 summarizes the improvements in antibacterial efficacy achieved through the encapsulation of vancomycin and gentamicin in PLGA/DOTAP nanoparticles against MRSA USA300. In their free forms, gentamicin exhibited greater intrinsic activity than vancomycin. Encapsulation reduced the minimum inhibitory concentration (MIC) of vancomycin by 16-fold (from 4 to 0.25 μg/mL) and gentamicin by more than 30-fold (from 2 to <0.063 μg/mL). Similar trends were observed for the minimum bactericidal concentration (MBC) and minimum biofilm bactericidal concentration (MBBC) values, with vancomycin showing reductions of at least 32-fold and gentamicin 16-fold compared to their free forms. Blank nanoparticles exhibited no antibacterial activity, confirming that the observed effects were solely due to the encapsulated drugs.

Table 2. MIC, MBC, and MBBC of Free and PLGA/DOTAP-Encapsulated Antibiotics against MRSA USA300[a]

formulations	MIC (μg/mL)	MBC (μg/mL)	MBBC (μg/mL)
free vancomycin	4	>64	>512
vancomycin in PLGA/DOTAP NPs	0.25	0.50	16
free gentamicin	2	4	64
gentamicin in PLGA/DOTAP NPs	<0.06	0.25	4
PLGA/DOTAP (blank control)	>1016	>1016	>7529

[a]All experiments were conducted using DMEM growth media at 37 °C with 5% CO_2 and n = 3. MIC and MBC were examined using a starting bacterial density of 8×10^6 cells/mL. MBBC was determined based on a 24 h preformed biofilm model.

The enhanced efficacy is likely due to the positively charged surface of the PLGA/DOTAP nanoparticles, which promotes electrostatic interactions with the negatively charged bacterial cell membranes and biofilm matrix. These interactions may facilitate improved drug delivery and penetration into bacterial cells and biofilms. Additionally, the sustained release properties of the nanoparticles may help maintain therapeutic drug concentrations over time, further enhancing their efficacy.

Anti-Intracellular Pathogen Activity of LPN Formulations in RAW-Blue and HaCaT Cells. Intracellular pathogens can evade traditional antibiotic treatments by residing and replicating within host cells. These pathogens are protected from antibiotics due to several vital challenges:[28] (i) most antibiotics are highly hydrophilic, preventing effective penetration across cellular membranes; (ii) intracellular accumulation is limited by efflux pumps that transport

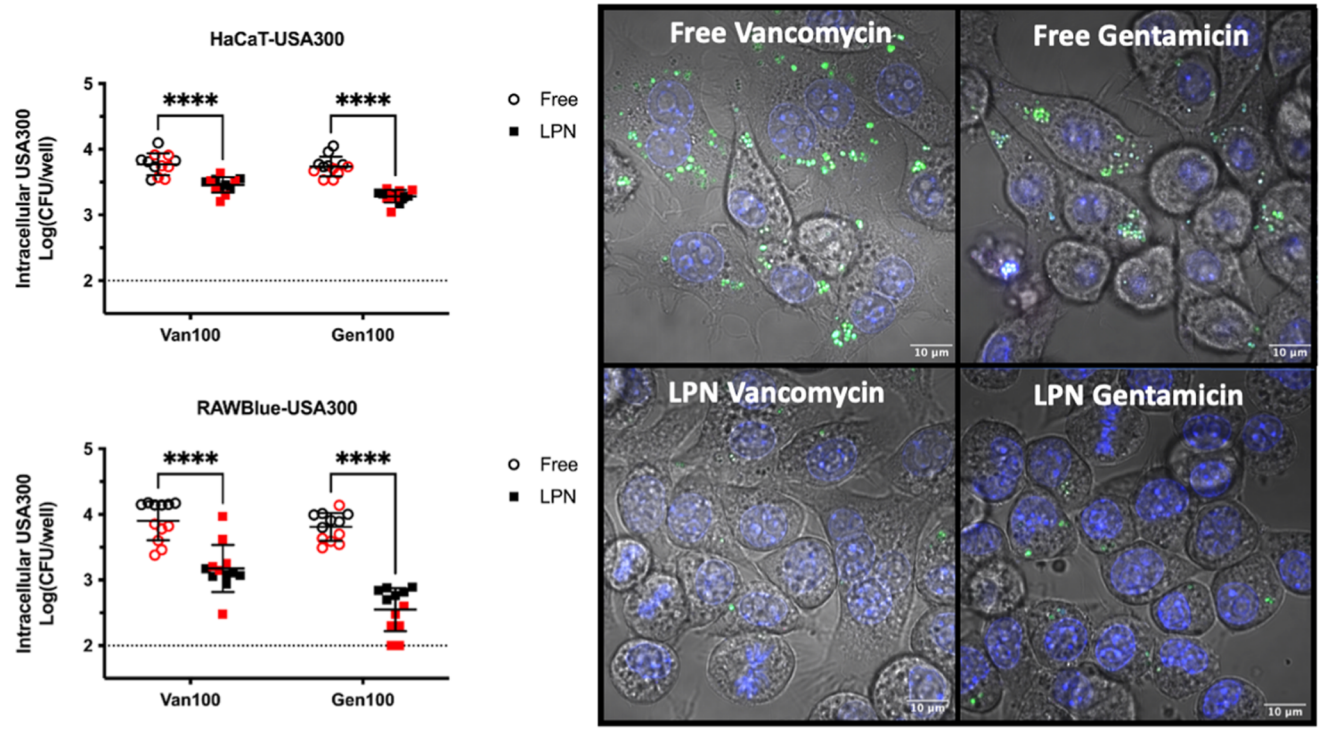

Figure 2. *In vitro* anti-intracellular pathogen activity of free and LPN-encapsulated antibiotics at 100 μg/mL. Left panel: intracellular MRSA USA300 recovered from HaCaT (top)/RAW-Blue (bottom) cells after antibiotic treatment for 24 h. Black and red colors represent two independent experimental replicates, each with six technical replicates. Error bars represent mean ± SD. Statistical significance was determined using multiple t tests with the Holm-Sidak correction (alpha = 0.05) with ****$p < 0.0001$. Right panel: CLSM images demonstrating intracellular killing of MRSA USA300 GFP by free antibiotics and LPN formulations in RAW-Blue macrophages. Nuclei were stained with DAPI (blue), and bacterial cells are shown in green fluorescence.

https://doi.org/10.1021/acsinfecdis.4c01016
ACS Infect. Dis. XXXX, XXX, XXX−XXX

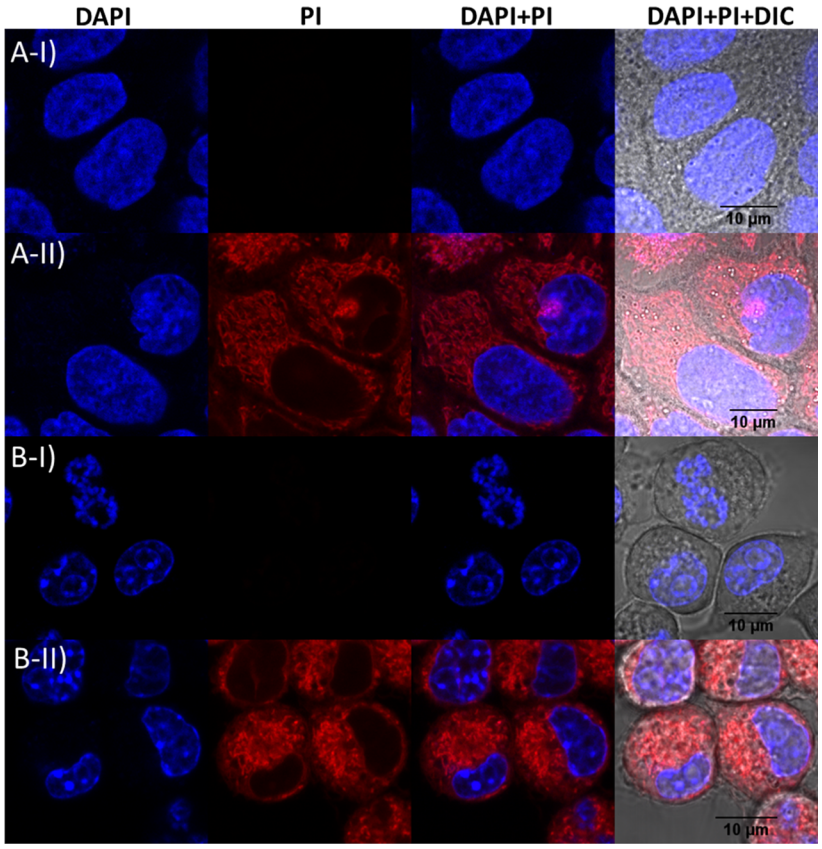

Figure 3. Comparative cellular uptake of free (I) or PLGA/DOTAP-encapsulated (II) PI by HaCaT (A) or RAW-Blue (B) cells. Cells were coincubated with PI (red, 5 μM) and DAPI nuclear stain (blue, 8 μg/mL) for 1 h at 37 °C, 5% CO_2 prior to imaging by CLSM. DIC: differential interference contrast image showing cell morphology.

antibiotics from the cell; and (iii) the harsh acidic and hydrolytic conditions within mature lysosomes can deactivate antibiotics that do gain entry. This is particularly relevant for antibiotics like gentamicin which, despite showing potent activity against MRSA (Table 2), has limited clinical utility against intracellular infections due to its poor membrane permeability. Carrier systems like LPNs offer an opportunity to repurpose such effective antibiotics by enabling their delivery across cellular membranes.

Using an established gentamicin protection assay to create an intracellular infection model,[29] we evaluated the ability of LPN-encapsulated antibiotics to overcome cellular barriers. Human keratinocyte (HaCaT) and murine macrophage (RAW-Blue) were infected with MRSA USA300 and treated with 100 μg/mL antibiotic formulations. This concentration was selected based on preliminary cytotoxicity studies demonstrating a therapeutic window where the LPN-encapsulated drugs were nontoxic, but free drugs were ineffective at killing intracellular bacteria.

Colony-forming unit (CFU) counts demonstrated the enhanced intracellular killing of LPN-formulations compared to the unencapsulated drugs, with approximately 0.3 Log and 0.45 Log reduction in intracellular bacteria in HaCaT cells for Van100 and Gen100, respectively (Figure 2). The enhancement was more pronounced in RAW-Blue macrophages, bringing down intracellular bacterial loads 0.7 Log (Van100) and 1.3 Log (Gen100).

The enhanced intracellular antibacterial efficacy of the LPN-antibiotic formulations observed in RAW-Blue macrophages, as compared to HaCaT keratinocytes, may be attributed to the intrinsic microbicidal mechanisms[30] of macrophages. This hypothesis is supported by confocal laser scanning microscopy (CLSM) data shown in Figure S1, which indicates that the cellular uptake of LPN-encapsulated propidium iodide (LPN-PI) was comparable between HaCaT and RAW-Blue cells. Orthogonal projections confirmed successful nanoparticle internalization, predominantly localized within the cytoplasm of both cell lines, with similar fluorescence intensity, particle-like morphology, and intracellular distribution patterns. Upon exposure to the encapsulated antibiotics released from the internalized nanoparticles, these microbicidal mechanisms may synergistically contribute to the effective eradication of intracellular pathogens.

To further visualize the enhanced intracellular antibacterial efficacy, confocal microscopy imaging was employed to investigate the intracellular survival of the green fluorescent protein (GFP)-expressing MRSA USA300 (Figure 2). Significant reductions in bacterial fluorescence were observed in RAW-Blue macrophages treated with the LPN-encapsulated antibiotics, as compared to the free antibiotic controls, corroborating the quantitative CFU data and confirming the potent intracellular killing efficacy of the LPN formulations.

Cellular Uptake and Intracellular Delivery of LPN-Encapsulated Antibiotics. To investigate whether LPNs could facilitate intracellular delivery of encapsulated antibiotics, we used the membrane-impermeable dye propidium iodide (PI) as a fluorescent probe (Figure 3). PI is excluded from living cells but readily enters and binds to nucleic acids upon membrane disruption, emitting bright red fluorescence. No intracellular fluorescence was observed when free unencapsu-

https://doi.org/10.1021/acsinfecdis.4c01016
ACS Infect. Dis. XXXX, XXX, XXX−XXX

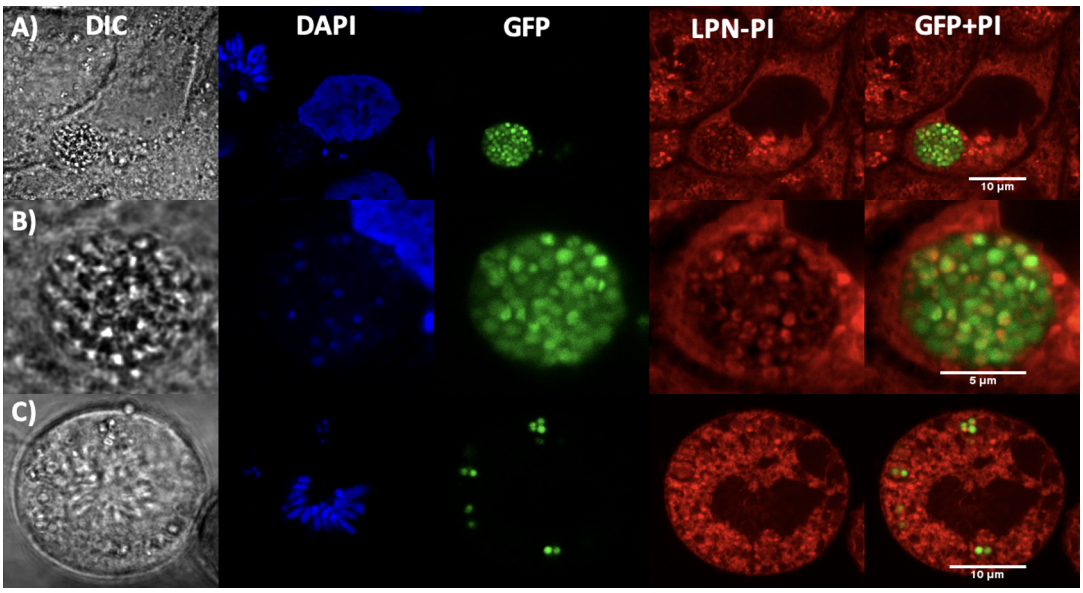

Figure 4. Cellular uptake of PLGA/DOTAP-encapsulated PI (red) by human keratinocytes HaCaT at different magnifications (A,B) or mouse macrophage RAW-Blue (C) after being infected by MRSA USA300 GFP (green). A and B show the same cellular uptake of PI in HaCaT cells, with 4B providing a higher magnification view to highlight detailed cellular localization. Both cell lines were coincubated with PI at 5 μM and DAPI (blue) at 8 μg/mL for 1 h at 37 °C, 5% CO_2 before CLSM imaging.

lated PI was coincubated with RAW-Blue and HaCaT cell lines, confirming its inability to permeate intact plasma membranes via diffusion or induce nonspecific endocytic uptake. In contrast, cells treated with LPN-encapsulated PI exhibited a significant increase in intracellular red fluorescence compared to free PI groups. Importantly, the enhanced intracellular delivery was specifically attributed to successful encapsulation rather than the mere presence of LPNs, as demonstrated in Figure S2, where physical mixing of blank LPNs with PI showed no enhancement in cellular uptake of PI. To compare the efficacy of intracellular PI delivery, PLGA-PI and LPN-PI formulations were evaluated in two nonprofessional phagocytic cell lines: 3T3 mouse fibroblasts and HaCaT keratinocytes. These cell types were chosen because nonprofessional phagocytes present greater challenges for intracellular delivery compared to professional phagocytes (Figure S3). The results indicated that LPN-PI exhibited enhanced proficiency in mediating the transport of PI into the cytoplasm. This substantial enhancement in cytosolic PI delivery demonstrates LPNs' capacity to facilitate cellular entry and endosomal escape of the encapsulated cargo.

After ascertaining LPNs' ability to enter both cell lines, the following question was how the nanoparticles trafficked intracellularly. If LPNs cannot access bacterial-containing compartments or release antibiotics into the cytosol where pathogens reside, the enhanced particle uptake would not translate to improved therapeutic outcomes, especially for dose-dependent bactericidal agents like gentamicin.[31] To investigate the intracellular trafficking of MRSA and LPNs, RAW-Blue and HaCaT cells were infected with GFP-expressing MRSA USA300. Following the removal of extracellular bacteria, LPN-encapsulated PI was added, and localization was analyzed using confocal microscopy. MRSA was observed within vacuoles, while LPN-PI was predominantly localized in the cytosol. LPN-PI was colocalized with internalized MRSA within the same vacuolar compartments, effectively coating/blanketing the intracellular pathogens (Figure 4). These images demonstrated that LPNs could access and effectively surround intracellular bacterial reservoirs. Furthermore, the cytosolic distribution of LPNs enabled targeting of pathogens that had escaped from initial membrane-bound vesicles. This capacity for both cellular entry and cytosolic release highlights the potential of LPNs to enhance antibiotic delivery to key intracellular sites of bacterial sequestration.

In Vivo Evaluation of LPN-Van in a Murine Skin Wound Model of Biofilm Infection. Prior to in vivo studies, the cytotoxicity of free and LPN-formulated gentamicin and vancomycin was evaluated using a lactate dehydrogenase (LDH) assay in HaCaT and RAW-Blue cells (Figure S4). Blank LPNs did not compromise membrane integrity in either cell line. For HaCaT cells, all antibiotic formulations exhibited >75% viability across the concentration range tested. RAW-Blue cells were more susceptible to gentamicin than vancomycin, with LPN-Gen and free Gen showing ~75% viability at a concentration of 15.6 μg/mL. In contrast, LPN-Van reduced viability below 75% only at 1000 μg/mL. An LPN-Van concentration of 500 μg/mL, based on this in vitro cytotoxicity profile, was selected as a safe and potentially therapeutic dose for subsequent in vivo studies.

Chronic wound infections, particularly those involving MRSA biofilms, are notoriously difficult to treat due to the resilience of these surface-attached communities. MRSA biofilms are also implicated in catheter colonization, prosthetic infections, osteomyelitis, and other persistent illnesses.[32] To evaluate the in vivo therapeutic efficacy of LPN-Van, we treated MRSA biofilms in a previously characterized excisional mouse skin wound model.[33,34] MRSA USA300 biofilms were developed through direct inoculation on the wounds for 24 h. These preformed biofilms were then treated topically for 24 h with 500 μg/mL LPN-Van. An equimolar concentration of free unencapsulated vancomycin, blank LPN vehicles, or water, were added to wounds on separate mice as controls. Post 24 h,

https://doi.org/10.1021/acsinfecdis.4c01016
ACS Infect. Dis. XXXX, XXX, XXX−XXX

wounds were excised and enumerated for bacterial burden via CFU quantification.

LPN-Van treatment (Figure 5) significantly reduced MRSA biofilm viability compared to untreated controls, achieving

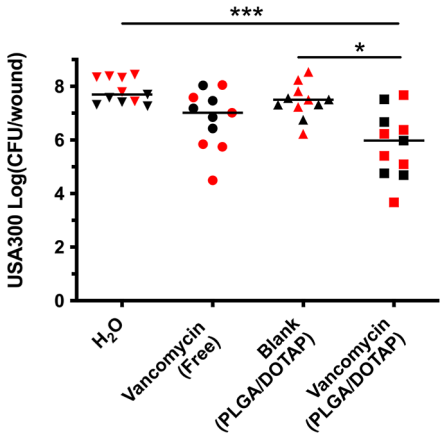

Figure 5. *In vivo* evaluation of LPN-Van (500 μg/mL) in a biofilm murine skin wound infection model. Wounds were inoculated with 10^4 CFU of USA300 for 24 h before treatment with the respective compounds. A dressing containing a metallic disk was applied on the wounds postaddition of compounds to restrict the compound exposure to the wound site. Wounds were then harvested 24 h postcompound exposure for CFU enumeration. Each data point represents CFU/wound from one mouse assessed on nonselective TSA plates, with the median values indicated by bars. Data were compiled from two independent experiments containing six (first experiment; red symbols) or five animals (second experiment; black symbols) per treatment group. Statistical analysis was performed using the nonparametric Kruskal–Wallis test with Dunn's post ad hoc test for intergroup comparisons. All pairwise comparisons were performed, and only statistically significant differences are annotated with asterisks (*p < 0.05, ***p < 0.001). The absence of annotations indicates no significant differences between groups.

98% eradication based on median values (p < 0.001). In contrast, free vancomycin achieved a 79.2% reduction in biofilm viability compared with the control, but this decrease was not statistically significant. The high bacterial counts in the Free Van group, reflect its reduced efficacy against biofilm-associated bacteria. The negative control group confirmed that MRSA USA300 thrived in the wound environment, reaching high cell densities of 10^8 CFU/wound. This underscores the resilience of bacteria in biofilm infections, where physiologically diverse subpopulations, including those with lower metabolic activity,[35,36] can withstand antibiotic treatments. Such adaptations limit the performance of LPN-Van in this biofilm setup.[37] Combining antibiotics with metabolic stimuli offers a promising strategy to overcome these challenges. Studies have shown that supplementing carbon sources and electron acceptors can potentiate antibiotics, even in cases of previously failed treatments.[36,38,39] LPNs, with their capacity to encapsulate both hydrophilic and hydrophobic compounds, offer a potential platform for codelivering antibiotics and metabolic stimuli. This approach could help overcome biofilm resilience and achieve better therapeutic outcomes in future studies.

Prophylactic Efficacy of LPN-Van in a Murine Skin Wound Infection Model. The efficacy of LPN-Van was also tested for its prophylaxis capability, i.e., preventing infection or disease before it occurs. Prophylactic treatments are commonly employed in medical settings to reduce the risk of infection, particularly when the risk is elevated, such as after surgery or in immunocompromised patients. In wound care, such treatments aim to prevent the colonization and proliferation of bacterial pathogens in wounds, which could lead to severe infections and complications. Therefore, we evaluated the prophylactic efficacy of LPN-Van in a skin wound model. Treatment of wounds 24 h prior to a single exposure with 500 μg/mL LPN-Van significantly reduced wound bacterial counts (Figure 6) compared to nontreated controls (p < 0.0001),

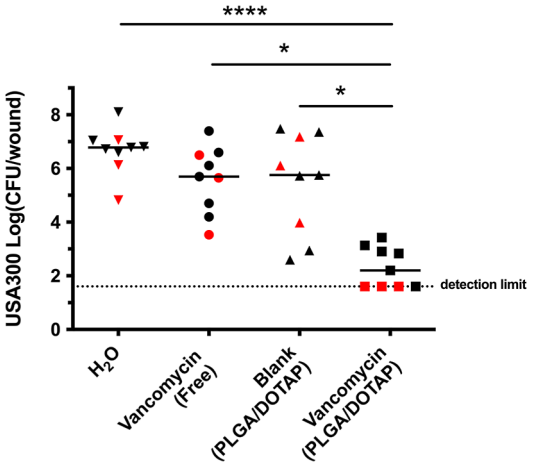

Figure 6. *In vivo* evaluation of LPN-Van (500 μg/mL) in a prophylactic murine skin wound model. Wounds were treated with the indicated compounds for 24 h together with the inoculation of 10^4 CFU of USA300. Dressing containing a metallic disk was applied on the wounds postaddition of compounds to restrict the compound exposure to the wound site. Wounds were then harvested 24 h postbacterial inoculation for CFU enumeration. Each data point represents CFU/wound from one mouse assessed on nonselective TSA plates, with the median values indicated by bars. Data were compiled from two independent experiments containing three (first experiment; red symbols) or six animals (second experiment; black symbols) per treatment group. Statistical analysis was performed using the nonparametric Kruskal–Wallis test with Dunn's post ad hoc test for intergroup comparisons. All pairwise comparisons were performed, and only statistically significant differences are annotated with asterisks (*p < 0.05, ****p < 0.0001). The absence of annotations indicates no significant differences between groups.

lowering CFUs close to the detection limit. In contrast, free unencapsulated vancomycin performed poorly at combating MRSA under these conditions, with no significant difference observed among water, free vancomycin, and blank LPN treatment groups. This stark divergence in antimicrobial activity highlights the inability of free vancomycin to penetrate infection sites effectively, corroborating previous reports on the poor transdermal delivery of hydrophilic antibiotics.[40] LPN-Van has shown enhanced penetration and antibiotic activity in skin wound models compared to free drug controls.

The potent prophylactic capability exhibited by the LPN formulation suggests they have the potential to be used as a coating material for medical transplants or to prevent surgical site infections. Moreover, the sustained release from LPN carriers could provide a localized depot for extended antimicrobial activity against newly invading pathogens at wound sites, a key advantage over conventional antibiotic therapy.[41,42] These in vivo results validate the ability of LPN platforms to drastically enhance vancomycin delivery and

https://doi.org/10.1021/acsinfecdis.4c01016
ACS Infect. Dis. XXXX, XXX, XXX−XXX

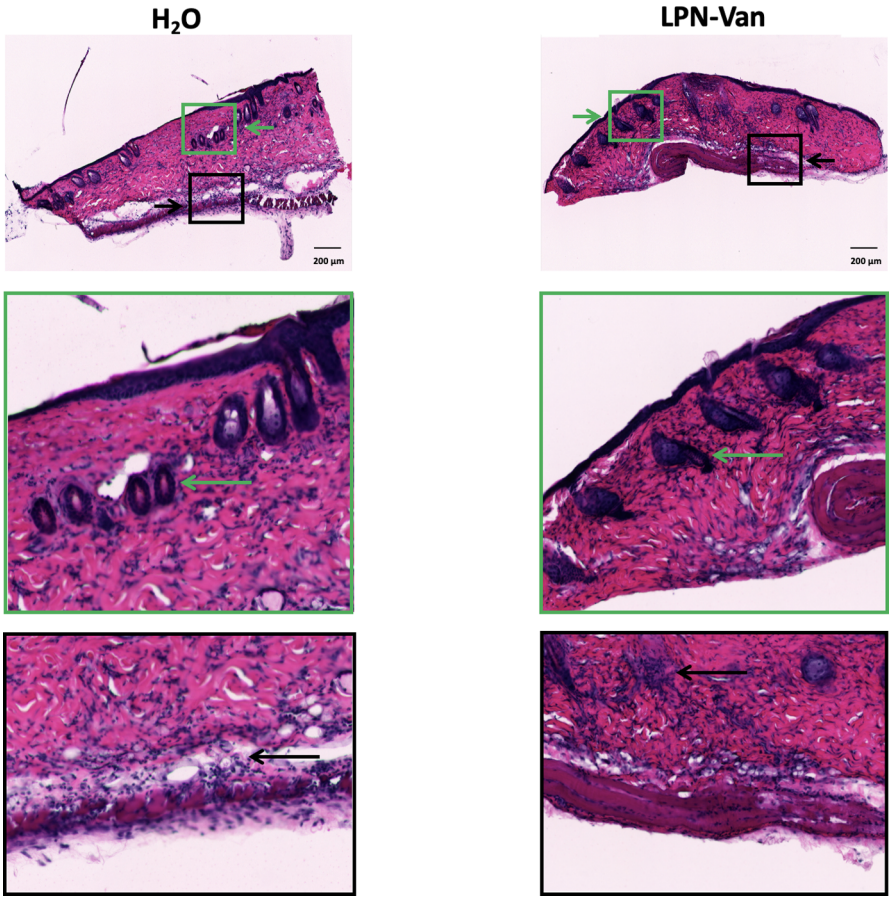

Figure 7. Representative histological images of wound tissue sections stained with hematoxylin and eosin (H&E) following 24 h treatment. Upper panels: low-magnification overview of tissue structure (scale bar: 200 μm). Middle and lower panels: Higher magnification (19.87×) of the green- and black-marked areas (upper panel), highlighting hair follicle integrity (green arrows) and inflammatory cell infiltration (black arrows), respectively.

efficacy in the treatment and prophylaxis of bacterial wound infections.

To determine whether LPN-Van exhibited any dermal toxicity on mouse skin, we inoculated uninfected punch-biopsy wounds with the same concentration used in the in vivo studies (500 μg/mL) and performed histological examination 24 h posttreatment. The histological analysis revealed an absence of necrosis and apoptosis in the LPN-Van treated skin samples (Figure 7). These findings suggest that LPN-Van exhibits no acute dermal toxicity at the tested therapeutic concentration and duration of exposure, indicating its suitability for topical administration.

CONCLUSIONS

In this study, LPNs composed of PLGA and DOTAP demonstrated efficient uptake by both phagocytic macrophages and nonphagocytic keratinocytes, enabling effective targeting of intracellular pathogens. At a concentration of 100 μg/mL, LPN-Van and LPN-Gen showed superior efficacy against intracellular MRSA in RAW-Blue and HaCaT cell lines compared to their free antibiotic counterparts. The strong in vitro anti-intracellular MRSA activity of LPN-encapsulated antibiotics laid the foundation for in vivo studies in a murine skin wound infection model. LPN-Van at a concentration of 500 μg/mL led to a significant reduction (98% removal) in biofilm bacterial loads compared to the water control, although no difference was detected between the free form and encapsulated antibiotics. The prophylactic effectiveness of LPN-Van was observed, effectively eradicating bacterial loads to levels near the detection limit, while free vancomycin was completely ineffective at the same dose. Importantly, the topical application of LPN-Van demonstrated no toxic effects in experimental mice based on histological analyses. These findings underscore the potential of LPN-based antibiotic delivery systems and pave the way for further investigations into adjuvant therapies, metabolism, and biodistribution studies for successful clinical translation.

METHODS

Materials. 1,2-Dioleoyl-3-trimethylammonium-propane chloride salt (DOTAP) was procured from Avanti Polar Lipids (Alabaster, AL, USA). PLGA (502H, MW 7000−17,000), poly(vinyl alcohol) (PVA, MW = 30−80 kDa, 87% hydrolyzed), vancomycin hydrochloride, gentamicin sulfate, dichloromethane (DCM), and paraformaldehyde (PFA) were acquired from Sigma-Aldrich. All staining dyes were purchased from Invitrogen (Thermo Fisher Scientific, USA). All other chemicals used in this study were of analytical grade and obtained from commercial sources.

Bacterial Strains and Mammalian Cell Cultures. MRSA USA300 and its GFP-expressing derivative were kindly provided by colleagues from Professor Kimberly Kline's laboratory.[43] The bacterial strains were cultured in tryptic soy broth (TSB) or on tryptic soy agar (TSA; 1.5% w/v)

https://doi.org/10.1021/acsinfecdis.4c01016
ACS Infect. Dis. XXXX, XXX, XXX−XXX

(Oxoid, UK) following standard maintenance protocols. The RAW-Blue, HaCaT, and 3T3 cell lines were maintained at 37 °C with 5% CO_2 in Dulbecco's modified Eagle medium (DMEM, Gibco, Life Technologies Limited, UK) supplemented with 10% fetal bovine serum (FBS, Life Technologies Limited, UK). For the RAW-Blue cell line, the medium was supplemented with Zeocin (InvivoGen) at a final concentration of 200 μg/mL.

PLGA/DOTAP Nanoparticle Fabrication and Characterization. The preparation of antibiotic-encapsulated LPNs was achieved via a modified emulsion−solvent−evaporation method.[23] Briefly, 4 mg of the selected antibiotic was dissolved in 0.5 mL of an aqueous 1% (w/v) PVA solution, followed by adding 2 mL of DCM containing 40 mg of PLGA. The primary emulsion was obtained by probe-sonicating the mixture at 50 W for 30 s. The primary emulsion was subsequently introduced dropwise into 10 mL of an aqueous PVA solution using a 25G needle. An additional sonication step of 60 s was performed to create a water-in-oil-in-water formulation. The nanoparticle suspension was then stirred for 4 h to facilitate DCM evaporation, followed by two centrifugation-resuspension cycles (20,000 *g*, 20 min, 4 °C) using deionized water.

Lipid coating was achieved using DOTAP, a cationic lipid, to develop the core−shell nanoparticle structure. A DOTAP thin-film was prepared by dissolving the lipid in DCM and subsequently evaporating the solvent under reduced pressure using a rotary evaporator. The thin-film was then hydrated directly with the nanoparticle suspension through gentle sonication. Following lipid coating, the nanoparticles were washed to remove excess lipid, and the resulting pellet was prepared for freeze-drying. The freeze-drying protocol consisted of overnight freezing at −80 °C, followed by lyophilization under vacuum for 48 h. The resulting freeze-dried nanoparticles were stored at −20 °C for subsequent use. Blank nanoparticles without antibiotics were prepared using an identical protocol, omitting the antibiotic during the primary emulsion preparation. For nanoparticles incorporating PI, the antibiotics were replaced with PI dissolved in dimethyl sulfoxide (DMSO). The resulting LPN-PI had a final concentration of 500 μM PI in 100 mg/mL LPN-PI.

For characterization, LPNs were dispersed in deionized water and loaded into disposable folded capillary cells (DTS1070). The mean particle size, PDI, and zeta potential were measured using a Zetasizer Nano ZS (Malvern, UK). Each sample was equilibrated for 30 s before measurement to ensure consistent results.

The drug loading and encapsulation efficiency were determined by analyzing residual antibiotic concentrations in the supernatants obtained during nanoparticle washing. Calibration curves were prepared using known concentrations of vancomycin and gentamicin dissolved in the supernatant of Blank-LNPs to account for potential interferences at each concentration. For vancomycin quantification, a high-performance liquid chromatography (HPLC) method was employed.[44] The analyte was separated on a C18 column (Zorbax SB, 5.0 μm, 4.6 mm × 250 mm) using a mobile phase of ultrapure water with 0.1% (v/v) acetic acid. The absorbance of vancomycin was measured at 282 nm for detection. Gentamicin quantification was performed using an aminoglycoside detection protocol.[45] Briefly, 50 μL of the gentamicin solution was added to a 96-well plate, followed by the addition of 50 μL of a mixture of reagent A (1 mL of 80 mg/mL *o*-phthalalldehyde in 95% ethanol) and reagent B (200 μL of 0.4 M boric acid, pH 9.7, 400 μL of 2-mercaptoethanol and 200 μL of diethyl ether). The fluorescence was measured at excitation and emission wavelengths of 360 and 460 nm, respectively, using a fluorometer (FLUO star Optima, BMG Labtech).

Different formulations' in vitro release profiles were evaluated using a dialysis bag technique. Dialysis bags (molecular weight cutoff of 7000 Da, Membra-Cel; Viskase Companies, Inc., Chicago, IL, USA) were filled with 10 mg of LPNs and immersed in either phosphate-buffered saline (PBS, pH 7.4, 20 mL) or TSB (pH 7.2, 20 mL) to mimic physiological and bacterial growth conditions, respectively. At predetermined time points, 5 mL of the release medium was collected and replaced with an equal volume of fresh medium. The amount of antibiotics released was quantified using the analytical methods described above.

Antibiotic Susceptibility Tests: MIC, MBC, and MBBC. *Planktonic Bacteria Assays.* The MIC and MBC against planktonic MRSA USA300 were determined using the broth dilution method, adapted from Wiegand et al.[46] An overnight culture of the USA300 strain was harvested, washed three times with PBS via centrifugation (8000*g*, 5 min) and resuspended in TSB to achieve an optical density (OD) of 0.8 at 600 nm, corresponding to approximately 2×10^8 CFU/mL. 2-fold serial dilutions of each antibiotic sample group, including both free antibiotics and those released from nanoparticles, were prepared in sterile 96-well plates, resulting in final antibiotic concentrations ranging from 0.063 to 64 μg/mL. The bacterial suspension was then added to each well to achieve a final inoculum of approximately 8×10^6 CFU/mL. Blank LPNs were included as a negative control to evaluate any intrinsic antibacterial activity of the nanoparticles and tested at significantly higher concentrations than the antibiotic-loaded nanoparticles to ensure any potential antibacterial effects from the carrier material could be detected. The 96-well plates were incubated overnight at 37 °C with 5% CO_2 for 24 h. Following incubation, the OD at 600 nm of each well was measured using a Tecan Microplate Reader M200. For MBC determination, selected wells were serially diluted and plated onto TSA plates. The MIC was defined as the lowest antibiotic concentration that inhibited observable bacterial growth or resulted in an $OD_{600} \leq 5\%$ of the untreated control sample after 24 h of exposure. The MBC was defined as the lowest antibiotic concentration required to completely eliminate planktonic USA300 cells, confirmed by the absence of bacterial colonies on TSA plates.

Biofilm Assays. To assess the MBBC, actively growing biofilms of MRSA USA300 were preformed in 96-well plates by inoculating 150 μL of bacterial culture at a final cell density of 8×10^6 CFU/mL. The plates were incubated for 24 h at 37 °C with 5% CO_2 to allow biofilm formation. Following incubation, the spent medium was carefully removed, and the biofilms were gently washed with PBS to eliminate planktonic bacteria. Serial dilutions of free or nanoparticle-encapsulated antibiotics in TSB, at final concentrations ranging from 2 to 512 μg/mL, were then added to the biofilms. Blank LPNs were also included as a negative control to evaluate any intrinsic antibiofilm activity of the nanoparticles, as described above. The plates were incubated for an additional 24 h under the same conditions (37 °C, 5% CO_2). After treatment, selected wells were serially diluted and drop-plated onto TSA plates to determine the MBBC. The MBBC was defined as the lowest antibiotic concentration required to completely eradicate

https://doi.org/10.1021/acsinfecdis.4c01016
ACS Infect. Dis. XXXX, XXX, XXX−XXX

biofilm-associated USA300 cells, as evidenced by the absence of bacterial colonies on TSA plates.

In Vitro Evaluation of Antibiotic-Loaded LPNs against Intracellular MRSA in HaCaT and RAW-Blue Cells. HaCaT keratinocyte cells were seeded in 6-well plates and cultured to approximately 80% confluency over 48 h, corresponding to ~8×10^5 cells per well. Live mammalian cell counts were determined by staining the cells with trypan blue and analyzing them using an automated cell counter (Invitrogen Countess II Automated Cell Counter, Thermo Fisher Scientific). Based on the counts of live cells, MRSA USA300 cells were prepared at a multiplicity of infection (MOI) of 100, allowing for standardization of the bacterial inoculum relative to the live mammalian cells. Following a 3 h coincubation to facilitate bacterial internalization, the supernatant was aspirated, and the cells were washed three times with PBS.

To establish intracellular infection, we employed the well-established gentamicin protection assay.[29,47] Gentamicin (500 μg/mL) was then supplemented for 1 h to kill extracellular bacteria while preserving intracellular bacteria, as gentamicin cannot penetrate mammalian cell membranes. After the gentamicin treatment, the medium was carefully removed using sterile glass tips connected to a vacuum pump, followed by three thorough washing steps with sterile PBS to ensure complete removal of extracellular gentamicin. The cells were then treated with LPN-encapsulated antibiotics for 20−24 h. Posttreatment, the mammalian cells were washed with PBS and lysed using 0.5 mL of trypsin and 0.2% Triton X-100 in PBS. The resultant lysates were serially diluted and plated on TSA to enumerate intracellular bacterial colonies.

RAW-Blue murine macrophage cells were seeded in 12-well plates and incubated for 48 h until reaching approximately 60% confluency (~5×10^5 cells per well). The infection, removal of extracellular bacteria, and antibiotic treatment steps followed a protocol similar to that used for HaCaT cells, with modifications to account for the fragility of RAW-Blue cells. Specifically, the MOI was set to 10, the infection time was limited to 1 h, and a single PBS wash was performed after infection to minimize cell disruption. Following the antibiotic treatment, the cells were washed with PBS and harvested by scraping in 1 mL of 1% Triton X-100 in PBS. The resulting lysates were serially diluted and plated on TSA to determine intracellular bacterial burdens.

In Vitro Cellular Uptake Studies and Confocal Microscopy Imaging. RAW-Blue and HaCaT cells were cultured in eight-well tissue-culture-treated chambers for 48 h to a confluency of 60% and 80%, respectively, prior to infection by USA300 GFP or treatment by PI-loaded LPNs. For cellular uptake of LPNs, the supernatant was removed and replaced with fresh media prior to the exposure of PI-loaded LPNs or free PI and DAPI in DMEM for 1 h. All cultures were visualized under a confocal laser scanning microscope (CLSM) (Zeiss LSM 780, Carl Zeiss Singapore). For labeling of intracellular MRSA, RAW-Blue and HaCaT cells were infected by USA300 GFP at MOI of 10 (1 h) and 100 (2 h), respectively, and the extracellular USA300 GFP were subsequently removed by gentamicin at 500 μg/mL for 1 h. The USA300 GFP-infected cultures were labeled by PI-loaded LPNs or free PI and DAPI in DMEM for 1 h before visualization using CLSM.

CLSM Imaging of LPN-Antibiotics-Treated Intracellular Pathogens. The RAW-Blue murine macrophage cell line was seeded at a density of 75,000 cells per well in an 8-well treated plate and allowed to be established for 24 h. Subsequently, the cells were infected with the GFP-expressing MRSA USA300 strain at an MOI of 10 for 1 h. The coculture was washed once with PBS, followed by adding gentamicin (500 μg/mL) for 1 h to remove extracellular bacteria. After this, 20 μL of the culture supernatant was removed and replaced with 20 μL of a 10-fold concentrated solution of either LPN-antibiotics or their free antibiotic counterparts. The treated cultures were then incubated at 37 °C with 5% CO_2 for 20 h. Following the incubation, the cells were labeled with PI and DAPI for 30 min before undergoing CLSM imaging.

In Vitro Cytotoxicity Evaluation in HaCaT and RAW-Blue Cell Lines. The cytotoxic effects of the free and LPN-encapsulated antibiotics were assessed using the LDH Cytoxicity Detection Kit (Clontech), following the manufacturer's instructions. LDH is a stable cytoplasmic enzyme released into the extracellular space upon cell membrane damage, and its activity in cell culture supernatants serves as a reliable marker for cytotoxicity.[48] The assay utilizes colorimetric detection, with the intensity of the resulting color measured at 490 nm, directly correlating to the number of damaged cells.[49]

Both cells were seeded into 96-well plates and incubated at 37 °C with 5% CO_2 for 48 h to allow for adherence and growth, reaching densities of 2.5×10^4 cells/well (HaCaT) and 1×10^4 cells/well (RAW-Blue). After incubation, the cells were gently washed three times with PBS. Fresh DMEM containing the test compounds was then added, and the cells were incubated for an additional 24 h under the same conditions. Following treatment, culture supernatants were collected and incubated with the LDH reaction mixture provided in the kit, and the absorbance was measured at 490 nm using a microplate reader (Tecan M200 PRO). Control conditions included a background control to measure LDH activity in the assay medium, a low control to quantify spontaneous LDH release from untreated cells, and a high control to assess maximal LDH release by treating cells with 1% Triton X-100. The percentage of cell viability was calculated as

$$\text{Viability (\%)} = \left(1 - \frac{\text{experiment value} - \text{low control}}{\text{high control} - \text{low control}}\right) \times 100$$

In Vivo Murine Skin Wound Infection Model. Animal experiments were conducted with the approval of the Institutional Animal Care and Use Committee (IACUC) under protocol ARF-SBS/NIE-A19061, in compliance with ethical guidelines for animal welfare. The murine wound infection model was modified based on established protocols described by Chong et al.[50] Male C57BL/6 mice (7−8 weeks old, 22−25 g; InVivos, Singapore) were used for the study. The mice were anesthetized with 3% isoflurane during the procedure to minimize pain and stress. The dorsal hair of the mice was removed using a two-step shaving procedure. This involved applying Nair cream (Church and Dwight Co.) followed by fine hair removal through shaving to ensure proper adhesion of the wound dressing. The skin was disinfected with 70% ethanol prior to wound creation. Full-thickness excisional wounds measuring 6 mm in diameter were created on the dorsal skin of the mice using a biopsy punch (Integra Miltex,

https://doi.org/10.1021/acsinfecdis.4c01016
ACS Infect. Dis. XXXX, XXX, XXX−XXX

New York). Following wound creation, 10 μL of OD-adjusted bacterial culture was applied to each wound, and the wounds were then sealed with a transparent dressing (Tegaderm, 3M) to prevent contamination and ensure consistent conditions.

For the prophylactic study, MRSA USA300 bacteria were cultured in TSB for 20 h at 37 °C under static conditions. After culturing, 10 μL of the OD-adjusted bacterial culture was added to each wound, together with 20 μL of treatment solutions, to achieve a final inoculum of 10^4 cells. Negative controls were included in this study, with wounds treated with 20 μL of sterile water to establish the baseline bacterial burden without any intervention. Blank LPNs were also used as vehicle controls to evaluate the effect of the carrier alone. Images of the wounds were taken after 24 h, and a 1 cm × 1 cm wound area was harvested and homogenized in 1 mL PBS. Serial dilutions of the homogenate were plated on nonselective TSA plates to determine CFU counts. For the biofilm study, OD-adjusted bacterial cultures were prepared as described above, but an inoculum of 10^6 cells/mL was used to establish biofilms. A 10 μL volume of the bacterial culture was added to each wound, and the wounds were sealed for 24 h to allow biofilm formation. After 24 h, 20 μL of treatment solutions were applied to the wounds, which were then resealed for an additional 24 h. In this study, negative controls (sterile water) and vehicle controls (blank LPNs) were also included to establish the baseline bacterial burden and evaluate the effect of the carrier, respectively. Imaging of the wounds was conducted before harvesting, and the wounds were homogenized and processed as described above for CFU enumeration.

Histological Analysis. Wound tissues were excised as described above[50] and fixed in 4% PFA prepared in 1× PBS (pH 7.4) at 4 °C for 24 h. Following fixation, the samples were cryoprotected by sequential immersion in 15% and 30% sucrose solutions (w/v) for 24 h each. The tissues were then embedded in Optimal Cutting Temperature (OCT) embedding medium (Sakura Finetek, California, USA) and frozen in liquid nitrogen. Thin cryosections (10 μm) were prepared using a Leica CM1860 UV cryostat (Leica Biosystems, Ernst-Leitz Strasse, Germany). The sections were sent to the Advanced Molecular Pathology Laboratory (Singapore) for H&E staining. For imaging, the H&E-stained slides were scanned at the A*STAR Microscopy Platform (AMP, Singapore) using a Brightfield MetaSystem Slide Scanner with a Zeiss AxioImager Z.2 microscope body and a 20×/0.8 NA objective (Carl Zeiss, Göttingen, Germany). The images were subsequently viewed and analyzed using VSViewer provided by AMP.

Statistical Analysis. All experimental results were analyzed using GraphPad Prism (version 8.0.2, San Diego, USA). As detailed in figure legends, ANOVAs, multiple t tests, and nonparametric analyses with p value corrections were conducted. Statistical significance critical values were defined as $^*p < 0.05$, $^{**}p < 0.01$, $^{***}p < 0.001$, and $^{****}p < 0.0001$.

■ ASSOCIATED CONTENT

Data Availability Statement

The data that support the findings of this study are openly available in NTU research data repository DR-NTU (Data) at 10.21979/N9/ARKJFG.

Supporting Information

The Supporting Information is available free of charge at https://pubs.acs.org/doi/10.1021/acsinfecdis.4c01016.

Figure S1 shows the cellular uptake of LPN-PI in HaCaT and RAW-Blue cells based on CLSM images; Figure S2 shows the cellular uptake study demonstrating that physical mixing does not enhance uptake of active compounds; Figure S3 shows labeling of 3T3 mouse fibroblasts and HaCaT human keratinocytes with PLGA-PI and LPN-PI; Figure S4 shows the cell viability of RAW-Blue and HaCaT cells after coincubating with different concentrations of free and LPN-formulated antibiotics (PDF)

■ AUTHOR INFORMATION

Corresponding Author

Say Chye Joachim Loo − *School of Materials Science and Engineering, Nanyang Technological University, Singapore 639798, Singapore; Singapore Center for Environmental Life Sciences Engineering, Nanyang Technological University, Singapore 637551, Singapore; Lee Kong Chian School of Medicine, Nanyang Technological University, Singapore 308232, Singapore;* orcid.org/0000-0001-5300-1275; Email: joachimloo@ntu.edu.sg

Authors

Wenrui Li − *School of Materials Science and Engineering, Nanyang Technological University, Singapore 639798, Singapore; NTU Institute for Health Technologies, Interdisciplinary Graduate Program, Nanyang Technological University, Singapore 637335, Singapore;* orcid.org/0000-0003-2509-945X

Chuan Hao Tan − *Singapore Center for Environmental Life Sciences Engineering, Nanyang Technological University, Singapore 637551, Singapore*

Jong-Suep Baek − *School of Materials Science and Engineering, Nanyang Technological University, Singapore 639798, Singapore*

Lai Jiang − *School of Materials Science and Engineering, Nanyang Technological University, Singapore 639798, Singapore*

Noele Kai Jing Ng − *Singapore Center for Environmental Life Sciences Engineering, Nanyang Technological University, Singapore 637551, Singapore*

Kelvin Kian Long Chong − *Singapore Center for Environmental Life Sciences Engineering, Nanyang Technological University, Singapore 637551, Singapore*

Jun Jie Wong − *Singapore Center for Environmental Life Sciences Engineering, Nanyang Technological University, Singapore 637551, Singapore;* orcid.org/0000-0002-9455-1051

Liheng Gao − *School of Electrical and Electronic Engineering, Nanyang Technological University, Singapore 639798, Singapore*

Kimberly A. Kline − *Singapore Center for Environmental Life Sciences Engineering and School of Biological Sciences, Nanyang Technological University, Singapore 637551, Singapore;* orcid.org/0000-0002-5472-3074

Complete contact information is available at: https://pubs.acs.org/10.1021/acsinfecdis.4c01016

Author Contributions

[¶]W.L. and C.H.T. contributed equally. C.H.T. conceived, planned, and carried out the experiments with the support from N.K.J.N. and W.R.L. L.J. and J.S.B. contributed to LPN

https://doi.org/10.1021/acsinfecdis.4c01016
ACS Infect. Dis. XXXX, XXX, XXX−XXX

fabrication and characterization. K.K.L.C., J.J.W., and L.H.G. contributed to the animal work and histological analysis. W.R.L. wrote the manuscript. C.H.T., S.C.J.L., and K.A.K. provided critical feedback and helped shape the research, analysis, and manuscript. All authors read and approved the final manuscript.

Funding

The authors would like to acknowledge the financial support from the Singapore Center for Environmental Life Sciences Engineering (SCELSE) (MOE/RCE: M4330019.C70), Ministry of Education AcRF-Tier 1 grant (RT08/19, RG79/22), the Singapore National Biofilm Consortium (SNBC/2021/SF2/P04), and the Singapore Food Agency (SFS_RND_SUFP_001_06).

Notes

The authors declare no competing financial interest.

During the preparation of this work, the authors used ChatGPT-4o and Anthropic's Claude to improve readability and language. After using the tools, the authors reviewed and edited the content as needed and take full responsibility for the content of the publication.

■ ACKNOWLEDGMENTS

The authors thank Lee Hiang Wee for providing technical details on the quantification of gentamicin and vancomycin, and Dr. Yu Hong for his insights into the design of the Table of Contents (TOC) graphic, which was created using BioRender.

■ REFERENCES

(1) Tong, S. Y.; Davis, J. S.; Eichenberger, E.; Holland, T. L.; Fowler, V. G., Jr. Staphylococcus aureus infections: epidemiology, pathophysiology, clinical manifestations, and management. *Clin Microbiol Rev.* **2015**, *28* (3), 603−661.

(2) Fraunholz, M.; Sinha, B. Intracellular Staphylococcus aureus: live-in and let die. *Front. Cell. Infect. Microbiol.* **2012**, *2*, 43.

(3) Pandey, S.; Sahukhal, G. S.; Elasri, M. O. The msaABCR Operon Regulates the Response to Oxidative Stress in Staphylococcus aureus. *J. Bacteriol.* **2019**, *201* (21), No. e00417.

(4) Li, M.; Cha, D. J.; Lai, Y.; Villaruz, A. E.; Sturdevant, D. E.; Otto, M. The antimicrobial peptide-sensing system aps of Staphylococcus aureus. *Mol. Microbiol.* **2007**, *66* (5), 1136−1147.

(5) Shimada, T.; Park, B. G.; Wolf, A. J.; Brikos, C.; Goodridge, H. S.; Becker, C. A.; Reyes, C. N.; Miao, E. A.; Aderem, A.; Götz, F.; Liu, G. Y.; Underhill, D. M. Staphylococcus aureus Evades Lysozyme-Based Peptidoglycan Digestion that Links Phagocytosis, Inflammasome Activation, and IL-1β Secretion. *Cell Host Microbe* **2010**, *7* (1), 38−49.

(6) Flannagan, R. S.; Kuiack, R. C.; McGavin, M. J.; Heinrichs, D. E. Staphylococcus aureus Uses the GraXRS Regulatory System To Sense and Adapt to the Acidified Phagolysosome in Macrophages. *mBio* **2018**, *9* (4), No. e01143.

(7) Foster, T. J.; Geoghegan, J. A.; Ganesh, V. K.; Höök, M. Adhesion, invasion and evasion: the many functions of the surface proteins of Staphylococcus aureus. *Nat. Rev. Microbiol.* **2014**, *12* (1), 49−62.

(8) Arciola, C. R.; Campoccia, D.; Speziale, P.; Montanaro, L.; Costerton, J. W. Biofilm formation in Staphylococcus implant infections. A review of molecular mechanisms and implications for biofilm-resistant materials. *Biomaterials* **2012**, *33* (26), 5967−5982.

(9) Roy, S.; Santra, S.; Das, A.; Dixith, S.; Sinha, M.; Ghatak, S.; Ghosh, N.; Banerjee, P.; Khanna, S.; Mathew-Steiner, S.; Ghatak, P. D.; Blackstone, B. N.; Powell, H. M.; Bergdall, V. K.; Wozniak, D. J.; Sen, C. K. Staphylococcus aureus Biofilm Infection Compromises Wound Healing by Causing Deficiencies in Granulation Tissue Collagen. *Ann. Surg.* **2020**, *271* (6), 1174−1185.

(10) Turner, N. A.; Sharma-Kuinkel, B. K.; Maskarinec, S. A.; Eichenberger, E. M.; Shah, P. P.; Carugati, M.; Holland, T. L.; Fowler, V. G., Jr. Methicillin-resistant Staphylococcus aureus: an overview of basic and clinical research. *Nat. Rev. Microbiol.* **2019**, *17* (4), 203−218.

(11) Liu, C.; Bayer, A.; Cosgrove, S. E.; Daum, R. S.; Fridkin, S. K.; Gorwitz, R. J.; Kaplan, S. L.; Karchmer, A. W.; Levine, D. P.; Murray, B. E.; Rybak, M. J.; Talan, D. A.; Chambers, H. F. Clinical Practice Guidelines by the Infectious Diseases Society of America for the Treatment of Methicillin-Resistant Staphylococcus aureus Infections in Adults and Children. *Clin. Infect. Dis.* **2011**, *52* (3), e18−e55.

(12) Yan, J.; Bassler, B. L. Surviving as a Community: Antibiotic Tolerance and Persistence in Bacterial Biofilms. *Cell Host Microbe* **2019**, *26* (1), 15−21.

(13) Garzoni, C.; Kelley, W. L. Return of the Trojan horse: intracellular phenotype switching and immune evasion by Staphylococcus aureus. *EMBO Mol. Med.* **2011**, *3* (3), 115−117.

(14) Jafernik, K.; Ładniak, A.; Blicharska, E.; Czarnek, K.; Ekiert, H.; Wiącek, A. E.; Szopa, A. Chitosan-Based Nanoparticles as Effective Drug Delivery Systems-A review. *Molecules* **2023**, *28* (4), 1963.

(15) Wang, Y.; Sun, H. Polymeric Nanomaterials for Efficient Delivery of Antimicrobial Agents. *Pharmaceutics* **2021**, *13* (12), 2108.

(16) Jiang, L.; Greene, M. K.; Insua, J. L.; Pessoa, J. S.; Small, D. M.; Smyth, P.; McCann, A. P.; Cogo, F.; Bengoechea, J. A.; Taggart, C. C.; Scott, C. J. Clearance of intracellular Klebsiella pneumoniae infection using gentamicin-loaded nanoparticles. *J. Controlled Release* **2018**, *279*, 316−325.

(17) Ferreira, M.; Pinto, S. N.; Aires-da-Silva, F.; Bettencourt, A.; Aguiar, S. I.; Gaspar, M. M. Liposomes as a Nanoplatform to Improve the Delivery of Antibiotics into Staphylococcus aureus Biofilms. *Pharmaceutics* **2021**, *13* (3), 321.

(18) Liu, W.; Ye, A.; Han, F.; Han, J. Advances and challenges in liposome digestion: Surface interaction, biological fate, and GIT modeling. *Adv. Colloid Interface Sci.* **2019**, *263*, 52−67.

(19) Ren, Y.; Nie, L.; Zhu, S.; Zhang, X. Nanovesicles-Mediated Drug Delivery for Oral Bioavailability Enhancement. *Int. J. Nanomed.* **2022**, *17*, 4861−4877.

(20) Alexis, F.; Pridgen, E.; Molnar, L. K.; Farokhzad, O. C. Factors affecting the clearance and biodistribution of polymeric nanoparticles. *Mol. Pharmaceutics* **2008**, *5* (4), 505−515.

(21) Hadinoto, K.; Sundaresan, A.; Cheow, W. S. Lipid−polymer hybrid nanoparticles as a new generation therapeutic delivery platform: a review. *Eur. J. Pharm. Biopharm.* **2013**, *85* (3), 427−443.

(22) Baek, J.-S.; Tan, C. H.; Ng, N. K. J.; Yeo, Y. P.; Rice, S. A.; Loo, S. C. J. A programmable lipid-polymer hybrid nanoparticle system for localized, sustained antibiotic delivery to Gram-positive and Gram-negative bacterial biofilms. *Nanoscale Horiz.* **2018**, *3* (3), 305−311.

(23) Tan, C. H.; Jiang, L.; Li, W.; Chan, S. H.; Baek, J.-S.; Ng, N. K. J.; Sailov, T.; Kharel, S.; Chong, K. K. L.; Loo, S. C. J. Lipid-Polymer Hybrid Nanoparticles Enhance the Potency of Ampicillin against Enterococcus faecalis in a Protozoa Infection Model. *ACS Infect. Dis.* **2021**, *7* (6), 1607−1618.

(24) Kamarehei, F.; Noori Saleh, G.; Hemmati, J.; Gohari, S. Newly designed nanoparticle-drug delivery systems against Staphylococcus aureus infection: a systematic review. *Int. J. Clin. Exp. Pathol.* **2024**, *17* (4), 96−107.

(25) Kim, S. W.; Lee, D.-G.; Choi, S.-M.; Park, C.; Kwon, J.-C.; Kim, S.-H.; Park, S. H.; Choi, J.-H.; Yoo, J.-H.; Shin, W.-S. Once-daily gentamicin administration for community-associated methicillin resistant Staphylococcus aureus in an in vitro pharmacodynamic model: preliminary reports for the advantages for optimizing pharmacodynamic index. *Yonsei Med. J.* **2010**, *51* (5), 722−727.

(26) Dinarvand, R.; Jafarzadeh Kashi, T.; Esfandyari-Manesh, M.; Marashi, S. M.; Samadi, N.; Atyabi, F.; Atyabi, F.; Eshraghin, S.; Dinarvand, R. Improved drug loading and antibacterial activity of minocycline-loaded PLGA nanoparticles prepared by solid/oil/water ion pairing method. *Int. J. Nanomed.* **2012**, *7*, 221−234.

https://doi.org/10.1021/acsinfecdis.4c01016
ACS Infect. Dis. XXXX, XXX, XXX−XXX

(27) Dinh, L.; Mahon, L.; Yan, B. Nano-Encapsulation and Conjugation Applied in the Development of Lipid Nanoparticles Delivering Nucleic Acid Materials to Enable Gene Therapies. *Appl. Nano* **2024**, *5* (3), 143−161. https://www.mdpi.com/2673-3501/5/3/11
(28) Maghrebi, S.; Joyce, P.; Jambhrunkar, M.; Thomas, N.; Prestidge, C. A. Poly(lactic-co-glycolic) Acid-Lipid Hybrid Microparticles Enhance the Intracellular Uptake and Antibacterial Activity of Rifampicin. *ACS Appl. Mater. Interfaces* **2020**, *12* (7), 8030−8039.
(29) Cheung, A. L.; Bayles, K. W. Tissue culture assays used to analyze invasion by Staphylococcus aureus. *Curr. Protoc. Microbiol.* **2007**, *4*, 9C41−9C47.
(30) Levin, R.; Grinstein, S.; Canton, J. The life cycle of phagosomes: formation, maturation, and resolution. *Immunol. Rev.* **2016**, *273* (1), 156−179.
(31) Mohamed, A. F.; Nielsen, E. I.; Cars, O.; Friberg, L. E. Pharmacokinetic-pharmacodynamic model for gentamicin and its adaptive resistance with predictions of dosing schedules in newborn infants. *Antimicrob. Agents Chemother.* **2012**, *56* (1), 179−188.
(32) Hassoun, A.; Linden, P. K.; Friedman, B. Incidence, prevalence, and management of MRSA bacteremia across patient populations-a review of recent developments in MRSA management and treatment. *Crit. Care* **2017**, *21* (1), 211.
(33) Roche, E. D.; Renick, P. J.; Tetens, S. P.; Carson, D. L. A model for evaluating topical antimicrobial efficacy against methicillin-resistant Staphylococcus aureus biofilms in superficial murine wounds. *Antimicrob. Agents Chemother.* **2012**, *56* (8), 4508−4510.
(34) Antonoplis, A.; Zang, X.; Huttner, M. A.; Chong, K. K. L.; Lee, Y. B.; Co, J. Y.; Amieva, M. R.; Kline, K. A.; Wender, P. A.; Cegelski, L. A Dual-Function Antibiotic-Transporter Conjugate Exhibits Superior Activity in Sterilizing MRSA Biofilms and Killing Persister Cells. *J. Am. Chem. Soc.* **2018**, *140* (47), 16140−16151.
(35) Gutierrez, A.; Jain, S.; Bhargava, P.; Hamblin, M.; Lobritz, M. A.; Collins, J. J. Understanding and Sensitizing Density-Dependent Persistence to Quinolone Antibiotics. *Mol. Cell* **2017**, *68* (6), 1147−1154e3.
(36) Allison, K. R.; Brynildsen, M. P.; Collins, J. J. Metabolite-enabled eradication of bacterial persisters by aminoglycosides. *Nature* **2011**, *473* (7346), 216−220.
(37) Dufour, D.; Leung, V.; Lévesque, C. M. Bacterial biofilm: structure, function, and antimicrobial resistance. *Endod. Top.* **2010**, *22* (1), 2−16.
(38) Meylan, S.; Porter, C. B. M.; Yang, J. H.; Belenky, P.; Gutierrez, A.; Lobritz, M. A.; Park, J.; Kim, S. H.; Moskowitz, S. M.; Collins, J. J. Carbon Sources Tune Antibiotic Susceptibility in Pseudomonas aeruginosa via Tricarboxylic Acid Cycle Control. *Cell Chem. Biol.* **2017**, *24* (2), 195−206.
(39) Peng, B.; Su, Y. B.; Li, H.; Han, Y.; Guo, C.; Tian, Y. M.; Peng, X. X. Exogenous alanine and/or glucose plus kanamycin kills antibiotic-resistant bacteria. *Cell Metab.* **2015**, *21* (2), 249−262.
(40) Raina, N.; Rani, R.; Thakur, V. K.; Gupta, M. New Insights in Topical Drug Delivery for Skin Disorders: From a Nanotechnological Perspective. *ACS Omega* **2023**, *8* (22), 19145−19167.
(41) Adams, S. B., Jr.; Shamji, M. F.; Nettles, D. L.; Hwang, P.; Setton, L. A. Sustained release of antibiotics from injectable and thermally responsive polypeptide depots. *J. Biomed. Mater. Res., Part B* **2009**, *90B* (1), 67−74.
(42) Krasko, M. Y.; Golenser, J.; Nyska, A.; Nyska, M.; Brin, Y. S.; Domb, A. J. Gentamicin extended release from an injectable polymeric implant. *J. Controlled Release* **2007**, *117* (1), 90−96.
(43) Wong, J. J.; Ho, F. K.; Choo, P. Y.; Chong, K. K. L.; Ho, C. M. B.; Neelakandan, R.; Keogh, D.; Barkham, T.; Chen, J.; Liu, C. F.; Kline, K. A. Escherichia coli BarA-UvrY regulates the pks island and kills Staphylococci via the genotoxin colibactin during interspecies competition. *PLoS Pathog.* **2022**, *18* (9), No. e1010766.
(44) Lee, H. W.; Kharel, S.; Loo, S. C. J. Lipid-Coated Hybrid Nanoparticles for Enhanced Bacterial Biofilm Penetration and Antibiofilm Efficacy. *ACS Omega* **2022**, *7* (40), 35814−35824.
(45) Hill, M.; Twigg, M.; Sheridan, E. A.; Hardy, J. G.; Elborn, J. S.; Taggart, C. C.; Scott, C. J.; Migaud, M. E. Alginate/Chitosan Particle-Based Drug Delivery Systems for Pulmonary Applications. *Pharmaceutics* **2019**, *11* (8), 379.
(46) Wiegand, I.; Hilpert, K.; Hancock, R. E. W. Agar and broth dilution methods to determine the minimal inhibitory concentration (MIC) of antimicrobial substances. *Nat. Protoc.* **2008**, *3* (2), 163−175.
(47) Garzoni, C.; Kelley, W. L. Staphylococcus aureus: new evidence for intracellular persistence. *Trends Microbiol.* **2009**, *17* (2), 59−65.
(48) Korzeniewski, C.; Callewaert, D. M. An enzyme-release assay for natural cytotoxicity. *J. Immunol. Methods* **1983**, *64* (3), 313−320.
(49) I. Clontech Laboratories. LDH Cytotoxicity Detection Kit User Manual, 2007. http://radio.cuci.udg.mx/bch/EN/Manuals/LDH-INT_Clontech.pdf (accessed on: Dec 3, 2024).
(50) Chong, K. K. L.; Tay, W. H.; Janela, B.; Yong, A. M. H.; Liew, T. H.; Madden, L.; Keogh, D.; Barkham, T. M. S.; Ginhoux, F.; Becker, D. L.; Kline, K. A. Enterococcus faecalis Modulates Immune Activation and Slows Healing During Wound Infection. *J. Infect. Dis.* **2017**, *216* (12), 1644−1654.

https://doi.org/10.1021/acsinfecdis.4c01016
ACS Infect. Dis. XXXX, XXX, XXX−XXX